รหัสโครงการ SUT7-706-54-12-69

รายงานการวิจัย

การสร้างแบบจำลองทางคณิตศาสตร์เพื่อปรับปรุงสมรรถนะของการแยก
(Mathematical modeling to improve the performance of chemical separation operations equipment)

ได้รับทุนอุดหนุนการวิจัยจาก
มหาวิทยาลัยเทคโนโลยีสุรนารี

ผลงานวิจัยเป็นความรับผิดชอบของหัวหน้าโครงการวิจัยแต่เพียงผู้เดียว

รหัสโครงการ SUT7-706-54-12-69

รายงานการวิจัย

การสร้างแบบจำลองทางคณิตศาสตร์เพื่อปรับปรุงสมรรถนะของการแยก
(Mathematical modeling to improve the performance of chemical separation operations equipment)

คณะผู้วิจัย

หัวหน้าโครงการ

ศาสตราจารย์ ดร.เอเดรียน ฟลัด

สาขาวิชาวิศวกรรมเคมี

สำนักวิชาวิศวกรรมศาสตร์

มหาวิทยาลัยเทคโนโลยีสุรนารี

ได้รับทุนอุดหนุนการวิจัยจากมหาวิทยาลัยเทคโนโลยีสุรนารี ปีงบประมาณ พ.ศ. 2554

ผลงานวิจัยเป็นความรับผิดชอบของหัวหน้าโครงการวิจัยแต่เพียงผู้เดียว

สิงหาคม 2556

Acknowledgements

The section of the research concerning the solution mediated transformation presented in this report is based partly on the research of Lek Wantha while under my supervision.

บทคัดย่อ

การศึกษาวิจัยนี้ประสบผลสำเร็จในการสร้างแบบจำลองทางคณิตศาสตร์เพื่อใช้ทำนายอัตราการเปลี่ยนรูปผลึกโดยอาศัยสารละลายเป็นสื่อกลาง (solution mediated transformation) ของผลึกที่มีโครงสร้างผลึกมากกว่าหนึ่งแบบ และช่วยให้เข้าใจเรื่อง การเกิดการเปลี่ยนรูปผลึกโดยอาศัยสารละลายเป็นสื่อกลาง มากยิ่งขึ้น ผลการคำนวนที่ได้จากแบบจำลองนี้ได้นำมาเปรียบเทียบกับค่าจากการทดลองการเกิด การเปลี่ยนรูปผลึกโดยอาศัยสารละลายเป็นสื่อกลางของ อัลฟา-ดีแอล-เมทไธโอนีน (α-DL-methionine) ไปเป็นแกมมา-ดีแอล-เมทไธโอนีน (γ-DL-methionine) โดยเปรียบเทียบในส่วนของความเข้มข้นของเมทไธโอนีนที่เปลี่ยนแปลงไปตามเวลาและอัตราส่วนโดยมวลของผลึกทั้งสองแบบ เบื้องต้นนั้นตัวแปรต่างๆ ที่ใช้ในการสร้างแบบจำลองเจาะจงใช้เฉพาะที่สามารถวัดได้จากการทดลองเกี่ยวกับปรากฏการณ์ การโตของผลึก การเกิดผลึกใหม่ การละลายของผลึก และช่วงเวลาก่อนการเกิดผลึกของผลึกทั้งสองแบบ โดยไม่มีตัวแปรที่สร้างมาจากข้อมูลของการเปลี่ยนรูปผลึกโดยอาศัยสารละลายเป็นสื่อกลางมาเกี่ยวข้อง ซึ่งแบบจำลองที่สร้างขึ้นให้ผลการคำนวนไปในทิศทางเดียวกันกับข้อมูลที่ได้จากผลการทดลอง แต่ค่าอัตราการเปลี่ยนแปลงโครงสร้างของผลึกนั้นไม่ถูกต้อง จากการวิเคราะห์ผลที่ได้ทำให้ทราบว่าตัวแปรที่มีผลทำให้แบบจำลองและการทดลองให้ผลไม่เหมือนกันคือ ค่าคงที่ของอัตราการละลาย เนื่องจากเมื่อลองกำหนดตัวแปรที่เกี่ยวข้องกับข้อมูลการเกิดการเปลี่ยนรูปผลึกโดยอาศัยสารละลายเป็นสื่อกลาง เพิ่มลงไปแบบจำลองให้ผลออกมาดีมาก สำหรับเหตุผลของความคลาดเคลื่อนของแบบจำลองนั้นก็ได้วิเคราะห์และนำเสนอไว้ในงานวิจัยนี้แล้ว การศึกษาในส่วนที่สองเป็นการสร้างแบบจำลองทางคณิตศาสตร์ของหอกลั่นไอน้ำแบบเปิด เพื่อนำมาใช้หาปริมาณอัตราส่วนที่เหมาะสมในการป้อนกลับของของเหลวผลิตภัณฑ์ที่ได้หลังจากการกลั่นเข้าสู่หอกลั่น ในกรณีที่ต้องการออกแบบให้หอกลั่นมีขนาดเล็กที่สุด (จำนวนชั้นของหอกลั่นน้อยที่สุด) ซึ่งในเบื้องต้นนั่นคาดว่าจะสามารถสร้างสมการที่สามารถแก้ได้โดยง่าย แต่เมื่อสร้างสมการขึ้นมาสำเร็จ สมการที่ได้นั้นมีความซับซ้อนมาก จนไม่สามารถแก้โดยใช้ระบบวิธีการทางการวิเคราะห์ได้ อย่างไรก็ตามสมการที่ถูกสร้างขึ้นนี้สามารถแก้ได้โดยใช้ระบบวิธีการทางตัวเลขในทุกๆ สภาวะการทดลอง ซึ่งในรายงานนี้ก็ได้แสดงตัวอย่างการแก้สมการไว้ด้วย

Abstract

The current study has successfully produced a mathematical model that can be used to predict the rate of solution mediated transformation of polymorphs and also aid understanding of the phenomenon. The model results have been compared with experimental values of the solution mediated transformation of α-DL-methionine into γ-DL-methionine (time dependent methionine concentration and polymorph mass fraction results). Initially the parameters in the model were fitted based on experimental measurements of crystal growth kinetics, nucleation kinetics, dissolution kinetics and induction times for the two polymorphs; there were no parameters in the model that were fitted using solution mediated transformation data. This model showed the same trends as the experimental data, but the rate of transformation was not correct. Analysis of the results showed that the only parameter that could be responsible for the mismatch was the dissolution rate constant; when this result was fitted based on solution mediated transformation results then the fit was very good. Reasons for the mismatch are also discussed.

A second study was made of modeling open steam distillation columns in order to solve for the reflux ratio resulting in a minimum number of stages. It was hoped to be able to find an analytical solution to the problem, however while an equation could be found that gave the solution, the equation was very complex and could not be analytically solved. The equation could be solved numerically for any set of operating conditions, and example solutions are shown in this report.

Contents

Figures

Chapter I
Introduction

1.1 Background and Significance

Separation operations are among the most significant operations in the chemical process industries, which are highly significant for the Thai economy, since they include petroleum and petrochemical production, food industries, paints and pigment production, and other chemical production industries.

The two most significant separation operations in the chemical industry (in terms of numbers of products which require these operations in their processing) are distillation and crystallization. These processes also account for a significant proportion of the cost of processing the chemicals, and therefore a significant proportion of the cost of the products. Thus the ability to optimize the separation operations has great significance to the chemical process industry, and such optimization depends on simple but accurate mathematical models of the processes involved. In many cases (for instance for distillation columns operating at steady-state) satisfactory modeling of the systems has been long completed, however there is great need in work in optimization of the processes based on known mathematical models. In other processes (for instance competitive crystallization of polymorphs in a batch crystallizer) optimization is not yet possible because mathematical models for the process are not yet sufficiently accurate.

The current project aims to model and optimize the open-steam distillation process, where a mathematical model of the process exists however it has not yet been optimized to obtain a general solution for the optimum reflux ratio used. Another aim is to improve the mathematical modeling of batch crystallization in combination with the polymorph transformation process. An improved mathematical model could be used for process optimization.

1.2 Objectives

(1) To produce a model based on first principle models of mechanisms and continuity that can accurately model the crystallization of two polymorphs simultaneously, and include the solution mediated transformation of the less stable polymorph to the more stable polymorph.

(2) To produce a model that can model the relationship between the significant variables in an open steam distillation column, and to use the model to find the reflux ratio, the key optimizable parameter in the column operation, at which a particular column (based on its feed state and composition, top product composition, and percent recovery of solute component into the top product of the column) requires a minimum number of stages. For a distillation column using a reboiler the reflux ration that results in a minimum number of stages is R = infinity. However (despite the commonly held but naïve) view that the same reflux ratio will give the same result for open steam columns, it is easy to show that this view is incorrect. The real optimum reflux ratio is, however, unknown.

1.3 Scope and Assumptions of Work

1.3.1 Scope and assumptions of Solution Mediated Transformation (SMT) study

In the SMT study it has been assumed that there are only two polymorphs present in the crystallization vessel at any time, and that the unstable polymorph has crystallized first (as the Ostwald stability rule suggests). The kinetics for the underlying physical mechanisms (crystal growth, crystal nucleation, and dissolution) for each polymorph can be modeled using empirical physical models depending on the supersaturation as the driving force, models that are widely accepted. The models can be parameterized based on previous measurements of the process kinetics and fit the experimental data well.

1.3.2 Scope and Assumptions of the Open Steam Distillation Model

The model for the open steam distillation column is based on the constant molar overflow theory assumed in the McCabe-Thiele method of design. This assumption means that the molar flowrates (i.e. flowrate in units of mole/s) of both the liquid and vapor phases in the top and bottom sections of the column are constant values. In this study the steam injected into the bottom of the column is assumed to be saturated at the pressure of the column. Pressure drops inside the column are ignored. The constant molar overflow assumption is correct when the two species involved have essentially the same molar enthalpy of vaporization under the conditions of the distillation (which is almost always approximately true), the heat of solution in the liquid phase is small (again, this is common), and where there are no heat losses in the column.

In addition this study assumes that the vapor-liquid equilibrium can be modeled via a constant value of the relative volatility. This assumption is accurate in many distillation systems, however there are obvious exceptions to this, including the ethanol-water system.

1.4 Outcomes of the research

The research has led to better understanding an ability to model the SMT process. In addition it has shown where the limitations in the current models of the physical processes leads to inaccuracies in modeling, particularly the need to improve dissolution rate models at the very small levels of the undersaturation (or driving force for dissolution) that are present for the unstable polymorph under the conditions of the SMT. Further research work is evidently needed in these dissolution rate models in order to find an acceptable model at very small driving forces.

In addition, the research has provided details of how the reflux ratio for the minimum number of stages in an open steam distillation column can be found based on the variables and parameters in the system. Unfortunately it was not possible to find an analytical solution for the problem, however several sets of numerical solutions have been determined and given graphically.

Chapter II
Theory and Literature Review

2.1 Polymorphs

Polymorphs are different crystal structures of the same species. Polymorphism can occur for two reasons; the first is that a molecule may have the same conformation in the polymorphic forms but different packing (packing polymorphism) and the second is that different conformers of a molecule may occur in the different crystal structures (conformational polymorphism). Both forms of polymorph are relatively common, with a characteristic example of a packing polymorph being *p*-nitrophenol [1] and a characteristic example of a conformational polymorph being 1-(1,6-dithiahexyl)anthracene-9,10-dione [2].

Two or more polymorphs of a species may exist at a particular state (T,P), however only one polymorph can be stable at a particular state; all polymorphs appearing in a system other than the stable form are referred to as metastable polymorphs. This leads to a characterization for polymorphic systems: a system is known as a monotropic system if one particular polymorph is stable (has the lowest free energy) for all temperatures below the melting points of the polymorphs, and enantiotropic if there is one or more transition temperatures where the stable polymorph changes from one polymorphic form to another. Since crystallization is fundamentally a kinetic process, it is possible that a metastable polymorph will form before the stable polymorph begins to crystallize. If a metastable polymorph exists then it should transform into the stable polymorph in order to minimize the free energy of the system. Ostwald's rule of stages states that in a given system the least stable polymorph that can crystallize will crystallize first, and this is followed by successive phase transformations into the next least stable polymorph until the stable polymorphic form is reached. Thus the first form created has the largest free energy of any polymorphic form that can crystallize in the system and the form then converts step by step to the polymorph having the minimum free energy. The stable polymorph must also have a lower solubility than the metastable polymorphs, and thus the system also steps down from polymorphs having a larger solubility to the minimum solubility form. It should be strongly noted here that Ostwald's rule of stages is an empirical statement based on observations rather than a fundamental law, and that many exceptions to this rule have already been observed.

2.2 Solution Mediated Transformation

Solution mediated phase transformation (SMT) is a process where a polymorph transforms into a more stable polymorph with a solvent or solution playing some role in the mechanism of the transformation. Care must be taken to distinguish this mechanism from solid state transformation which tends to be a much slower process (at an equivalent temperature) due to the more constrained nature of the molecules in the solid state. Solution mediated phase transformation consists of three main mechanisms, the nucleation of the more stable polymorph, the growth of the more stable polymorph and the dissolution of the less stable polymorph. Thus the SMT can be modeled by a system that connects the fundamental models of these mechanisms in a rigorous way.

The method to connect the models of the fundamental phenomena in the SMT to an overall predictive model of the SMT is the population balance. The population balance model was independently derived by two groups in the 1960s, Hulbert and Katz [3] and Randolph and Larson [4,5]. Randolph and Larson [6] have stated that "… we shall develop a *predictive* multidimensional particle distribution theory …[which] is useful in the *a priori* prediction of the *form* and often the *magnitude* of the particle distribution" (where the highlights are those used by the original authors!). What is clear from this comment is that the population balance model was always intended as a *predictive* and *a priori* model. The parameters in the model (such as the growth rate as a function of supersaturation or the dissolution rate as a function of undersaturation), are easily measureable, and the boundary condition (the population density at zero size, which is equal to the birth rate at zero size divided by the growth rate at zero size for the supersaturation encountered) is also easily determined. The initial condition is the crystal size distribution of the contents of the vessel at the start of the crystallization, which is known. In order to fully model the SMT it is necessary to formulate a population balance equation for each of the polymorphs present in the system. Since the measurements and fundamental models required for the population balance model (nucleation, growth, and dissolution for each of the polymorphs) seem straightforward, it appears that a fully predictive model of SMT for a particular system should also be straightforward. The methods used for measurements of the underlying data required for the kinetics, and the models commonly used to fit the data, are available in well-known reference texts [7].

However, modeling of the SMT is essentially never done via a predictive method. In nearly all cases in the literature it is done by fitting the model parameters required in the underlying models for the crystal growth, nucleation, and possibly also dissolution kinetics, to experimental data for the SMT. Typical descriptions of methods include the following: "…the parameters of the kinetic equations were estimated using data sets of Run 1 and Run 2." [8]; "…the in-situ experimental data combined with parameter estimation algorithms were used to calculate the nucleation and growth kinetics …" [9]. This is not meant as a criticism of these previous studies (since these studies represent very good research concerning SMT) or other similar previous studies of the SMT.

2.3 Open Steam Distillation

Open steam distillation is a technique that is similar to ordinary distillation processes, however where instead of using a reboiler to produce vapor from the liquid at the bottom of the column, steam is injected directly into the bottom of the column. In this case all the liquid at the bottom of the column becomes the bottom product. Naturally this type of system is specific to processes where the bottom product of the column is intended to be predominately composed of water. This can be a more efficient process because plants typically have ready sources of steam (for heating and other purposes) and designing the column does not require the design or construction of the heat exchanger required for the reboiler. The types of design calculations for open steam columns are modifications of those required for traditional columns, taking into account the differences in the mass, component and energy balances in the bottom section of the column.

2.4 Objectives

(1) To produce a model of the solution mediated phase transformation of polymorphs based on first principles modeling, including continuity equations for particle numbers (i.e. the population balances for each polymorph) and measured kinetic values of the underlying process mechanisms (crystal growth, crystal nucleation, and crystal dissolution). The project will also compare the model to carefully determined experimental data for the SMT for α- and γ-DL-methionine, and industrially and biologically significant amino acid that crystallizes in a polymorphic system.

(2) To produce a model for the open steam distillation process for a binary feed mixture in terms of the significant variables and parameters in the system (for instance top

product composition, percent recovery, feed composition and state, relative volatility of the solute, etc…). This model is then to be analyzed mathematically in order to fins the reflux ratio at which a minimum number of theoretical stages will result.

Chapter III

Mathematical Models Used in the Study

3.1 Models used in the Solution Mediated Transformation Simulation

For the model of the crystallizer with SMT the first component of the model required is the population balance. This equation is an equation of continuity of entities (as in particles) and is given via a balance of particles within a differential size class (L to L + dL) into and out of a differential control volume, as shown in Fig. 3.1. The number density of particles within this size range is n (#/m^3.m). Velocity vector components are represented by v.

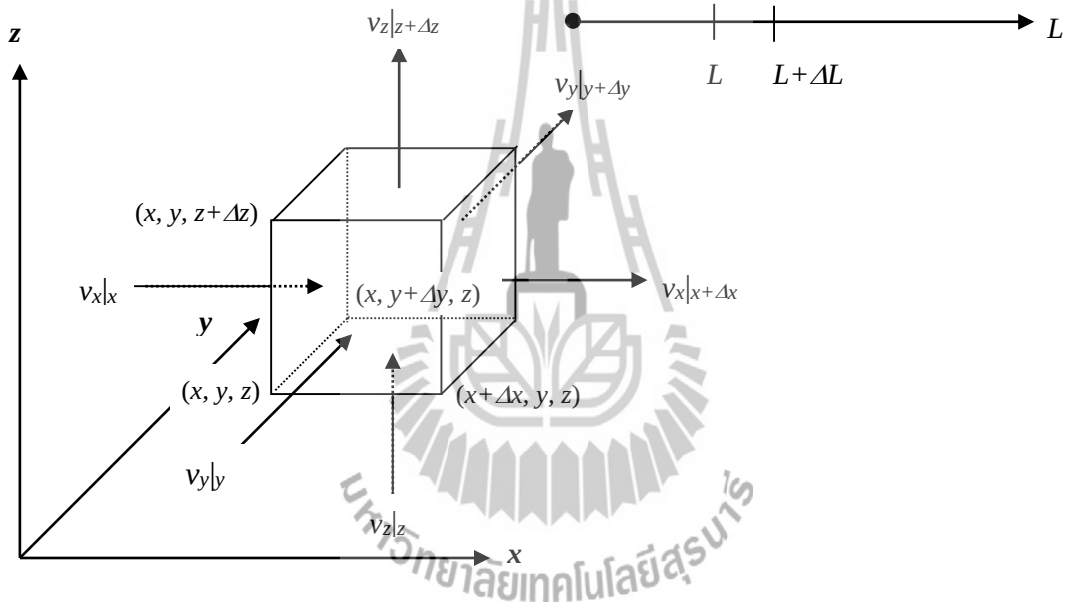

Fig. 3.1: Finite control region, consisting of a control volume and particle size range, for the derivation of the population balance.

The end result of this balance is the partial differential equation (PDE)

$$\frac{\partial n(x,y,z,L,t)}{\partial t} = -\left(\frac{\partial (v_x n)}{\partial x} + \frac{\partial (v_y n)}{\partial y} + \frac{\partial (v_z n)}{\partial z} + \frac{\partial (Gn)}{\partial L} \right) \tag{3.1}$$

or

$$\frac{\partial n}{\partial t} + \nabla \cdot (\mathrm{vn}) + \frac{\partial (Gn)}{\partial L} = 0 \tag{3.2}$$

This derivation did not, however, take into account mechanisms that could give rise to new crystals (birth) or those that could destroy entities (death). The nucleation of crystals is considered to occur at a size approaching zero, and hence can be taken care of using a boundary condition rather than as an extra term in the PDE. This equation is the well-known population balance equation (PBE)

$$\frac{\partial n}{\partial t} + \nabla \cdot (\mathrm{vn}) + \frac{\partial (Gn)}{\partial L} - B + D = 0 \tag{3.3}$$

In the case of the current research it is necessary to write this equation for each of the polymorphs, in this case polymorph α and polymorph γ. G is the crystal growth rate of the polymorph considered in the equation.

The equation above is impossible to solve except in a few cases. If the system is well mixed (i.e the properties of the system are the same at any point in the system) than it is possible to use a "well-mixed" form of this balance. This can be achieved by integrating the spatially dependent population balance above over the entire region V, and then simplifying the integral of the spatial divergence of the population flux to a surface integral using the Gauss-Ostrogradskii Divergence Theorem. The result is

$$\frac{\partial n}{dt} + n\frac{\partial (\log V)}{\partial t} + \frac{\partial (Gn)}{\partial L} = \sum \frac{Q_{in,i} n_{in,i}}{V} - \sum \frac{Q_{out,i} n_{out,i}}{V} + B - D \tag{3.4}$$

Here, the Q terms represent either in or out-flows with their respective particle number densities n_{in} or n_{out}. V is the volume of the crystallizer.

The crystallizer modeled in this work is a batch crystallizer. This is a more complex model than a continuous crystallizer, since continuous crystallizers operate at steady-state resulting in the first two terms being equal to zero. This reduces the continuous crystallizer models being ordinary differential equations: the assumptions for the batch crystallizer maintain the model as a PDE however. For the batch crystallizer there are no inflows or outflows, and in a carefully controlled batch we can assume that birth and death terms are also zero. In addition, when the change in volume of the species on crystallization is small (as is usually the case) a batch crystallizer operates at constant volume, and as such the second term on the left hand side is zero. In addition, the crystal growth rate is independent

of crystal size, such that (in the third term of the left hand side) *G* can be removed from the differential. Thus the model becomes (for the two polymorphs)

$$\frac{\partial n_\alpha}{\partial t} + G_\alpha \frac{\partial n_\alpha}{\partial L} = 0 \quad n_\alpha(L, t=0) = n_{\alpha,0} \quad n_\alpha(L=0, t) = B_\alpha(t)/G_\alpha(t) \tag{3.5}$$

$$\frac{\partial n_\gamma}{\partial t} + G_\gamma \frac{\partial n_\gamma}{\partial L} = 0 \quad n_\alpha(L, t=0) = n_{\alpha,0} \quad n_\gamma(L=0, t) = B_\gamma(t)/G_\gamma(t) \tag{3.6}$$

The driving forces for the crystallization processes are

$$S_\alpha(t) = \frac{C_\alpha(t)}{C_\alpha^*} \tag{3.7}$$

$$S_\gamma(t) = \frac{C_\gamma(t)}{C_\gamma^*} \tag{3.8}$$

These are different functions since the solubility (C*) of the two polymorphs are different. However the actual concentration of the two polymorphs is the same at any time (since the polymorph molecules are identical in the liquid phase). The growth rate *G*(*t*) and nucleation rate *B*(*t*) can be determined from the following models

$$G_\alpha(t) = k_{G,\alpha}(S_\alpha(t) - 1)^{n\alpha} \tag{3.9}$$

$$G_\gamma(t) = k_{G,\gamma}\left(S_\gamma(t) - 1\right)^{n\gamma} \tag{3.10}$$

$$B_\alpha(t) = k_{B,\alpha}\left(S_\alpha(t)\right)^{nb\alpha} \tag{3.11}$$

$$B_\gamma(t) = k_{B,\alpha}(S_\gamma(t))^{nb\gamma} \tag{3.12}$$

If the driving force for a polymorph is negative then the growth becomes dissolution. This can only occur to the less stable polymorph (in this case the alpha one).

$$D_\alpha(t) = k_{D,\alpha}(1 - S_\alpha(t))^{nd\alpha} \tag{3.13}$$

The model also contains an experimentally determined induction time; the time required from the creation of supersaturation until the creation of viable nuclei. The parameters in these kinetic models can be found from fitting sets of accurate experimental data. The kinetic data needed to parameterize the models for DL-methionine have already been collected in a set of previous articles.

3.2 Models Used in the Open Steam Distillation Model

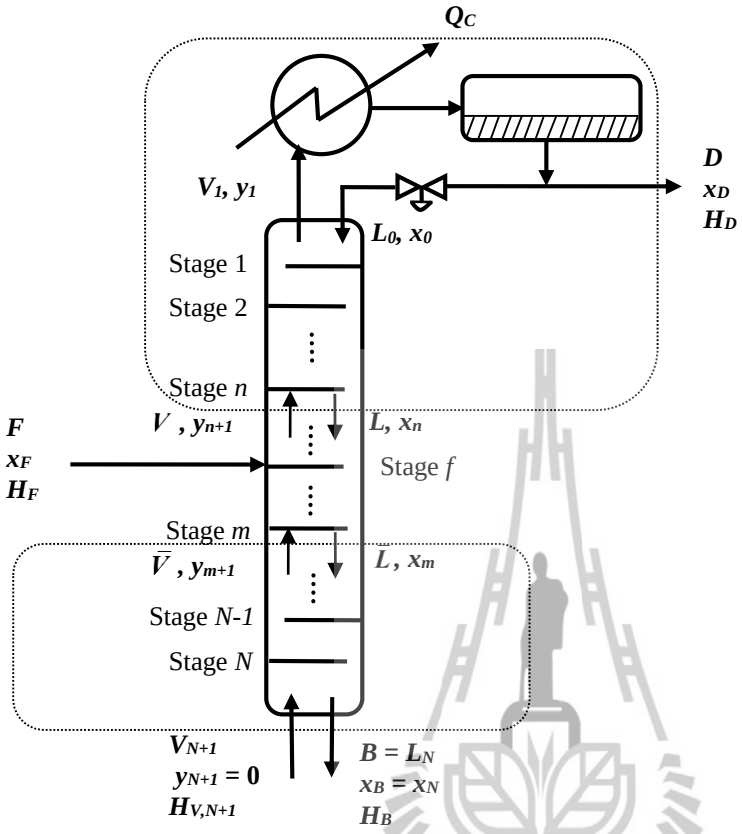

Fig. 3.2 Schematic diagram of an open steam distillation column showing all significant flows and compositions, and control volumes for the balances used.

A schematic diagram of the type of column used for open-steam distillation giving relevant solute mole fractions in stream flows (x for mole fractions in liquid streams and y for mole fractions in vapor streams) and the molar flow rates of the streams in kmol/s (L for liquid flows and V for vapor flows, with rates in the bottom section having an overscore) is given above. It is also necessary to do an energy balance over the entire column, and so enthalpy values (H) are given for inflows and outflows, as well as the cooling load in the condenser at the top of the column.

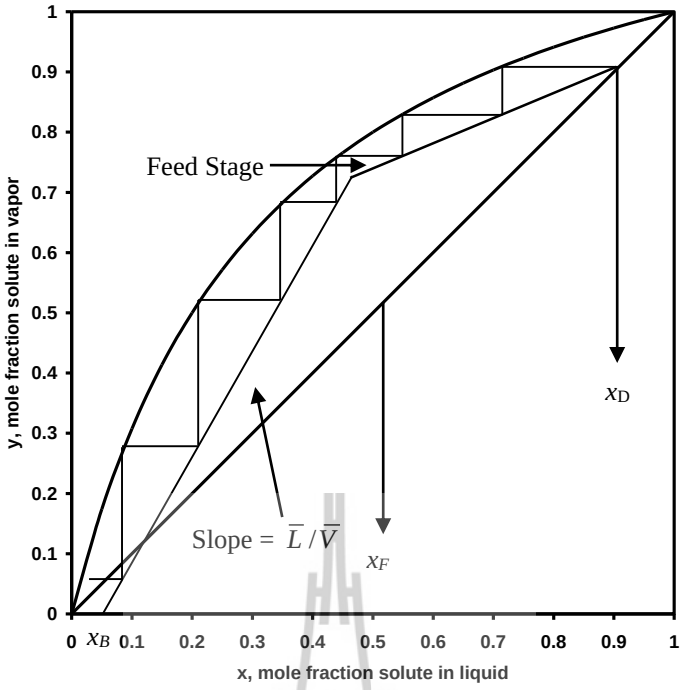

Fig. 3.3 Schematic diagram of the design of an open steam distillation column showing equilibrium and balance lines used.

Balances over the entire column give:

$$F + \overline{V}_{N+1} = D + B \tag{3.14}$$

$$Fx_F = Dx_D + Bx_B \tag{3.15}$$

The top section of the column can be modeled with a solute balance over a finite set of stages (from the top of the column to an arbitrary stage *n* in the top section, above the feed point).

$$y_{n+1} = \frac{L}{V}x_n + \frac{D}{V}x_D \tag{3.16}$$

Which reduces to

$$y_{n+1} = \frac{R}{R+1}x_n + \frac{x_D}{R+1} \tag{3.17}$$

Based on the definition of the reflux ratio, $R = L/D$ and the overall balance which shows that $V = L + D$.

The bottom section of the column is modeled with similar solute balances

$$y_{m+1} = \frac{\bar{L}}{\bar{V}} x_m - \frac{\bar{L}}{\bar{V}} x_B \tag{3.18}$$

The feed mixture must also be added at the most appropriate point of the column, which is determined via balances around the feed based on the following equation

$$y = \frac{q}{q-1} x - \frac{z_F}{q-1} \tag{3.19}$$

Where q is defined via the following equation involving the enthalpies of the saturated feed, saturated vapor and saturated liquid at the same temperature and pressure (or the fraction of the feed which is a liquid if the feed is a two-phase mixture).

$$\frac{\bar{L} - L}{F} = \frac{H_V - H_F}{H_V - H_L} = q \tag{3.20}$$

The q-line represents the locus of possible intersection points for the top section operating line and the bottom section operating line. This allows for the bottom section operating line to be fully specified given the top section operating line (which only requires the top product composition x_D and the reflux ratio R) and the q-line (which requires the feed composition z_F and enthalpy H_F).

In order to determine the driving force for the mass transfer at any stage in a column (or at any height in a packed column) the equilibrium concentrations must also be known, which is usually given as a function $y^* = f(x)$, where y^* is the equilibrium vapor phase mole fraction for a liquid phase mole fraction of x in the contacting liquid phase. The function depends on the thermodynamics in the given binary system, however a simple and commonly used assumption is that of constant relative volatility, α, where relative volatility is defined (in a binary system) as

$$\alpha = \frac{y^*/(1-y^*)}{x/(1-x)} \tag{3.21}$$

Solving to obtain the equilibrium vapor phase solute mole fraction gives

$$y^* = \frac{\alpha x}{1 + x(\alpha - 1)} \tag{3.22}$$

Thus, at a particular point in a column (a stage in a staged column, or at a particular point in the packing for a packed column) the equilibrium vapor phase in contact with the liquid phase is

$$y_n^* = \frac{\alpha x_n}{1 + x_n(\alpha - 1)} \tag{3.23}$$

Equation 3.23 is valid for the entire column, unlike equation 3.17 which is only valid for the section of the column above the feed, and equation 3.18 which is valid only for the section below the feed. Together, equations 3.17, 3.18, and 3.23 describe the driving force for the distillation, and also the separation that can be expected in one ideal stage, for the packed and staged columns. It should be noted that these equations are using only mass balances on sections of the columns and equilibrium thermodynamics, and hence the equations are equally valid for both types of columns.

Since the contacting methods are different in packed columns and staged columns, as is the required result (either the height of packing required or the number of stages required) the derivations for modeling the two types of column now begin to differ. However the reflux ratio for the minimum number of stages should be very close to the reflux ratio for the minimum height of packing. Starting with the packed column we can derive the height of packing required based on the mass transfer rates as a function of position in the column, a derivation which is given in many texts on mass transfer design. The height of packing for a particular section of column is given by the equation

$$L_T = \int_{y_1}^{y_2} \frac{d(Vy)}{K_y a S(y^* - y)} \tag{3.24}$$

Where y_1 represents the vapor phase mole fraction entering the bottom of the section, y_2 represents the vapor phase mole fraction leaving the top of the section, y^* is the equilibrium vapor phase composition (which depends on the liquid it is in contact with) and is given by equation 3.23, y is the actual vapor phase composition at that point and is given by equation 3.17 or 3.18 depending on whether the point is in the section above the feed point or the section below the feed point, V is the vapor phase flow rate (in mole/s or

similar), S is the packed cross-section of the column, and $K_y a$ represents a mass transfer coefficient (mole/m^{2}s) multiplied by a specific surface area for the packing (m^2 interfacial area/m^3 packed volume). The cross-section area is usually constant since constant diameter columns are usually used, and the vapor phase flow rate is also constant in a section based on the constant molar overflow assumption already made in deriving the mass balances. The assumption that the mass transfer coefficient and specific surface area of the packing are also constant leads to

$$L_T = \frac{V}{K_y a S} \int_{y_1}^{y_2} \frac{dy}{(y^* - y)} \tag{3.25}$$

The term outside the integral is usually referred to as the height of a transfer unit based on the overall gas phase driving force (H_{OG}), and the integral is referred to as the number of transfer units based on the overall gas phase driving force (N_{OG}). In order to determine the minimum height of packed column which could achieve a particular separation we would need to minimize the number of transfer units.

To calculate the number of transfer units in the distillation column it is necessary to sum two integrals, one for the section of column below the feed stage and one for the section of column above the feed stage.

The equilibrium line, equation 3.23 (which is valid for both sections) has only a single parameter which is known for any relevant system. The top section operating line contains only two parameters, the top product composition x_D and reflux ration R. The value of x_D is given in the problem statement as one of the two major design objectives of the column (along with the solute recovery, C_R). The value of R is what we can optimize in order to minimize the value of the number of transfer units. This indicates that in the top section of the column we know both functions in the integral, y^* and y. This does not indicate that we can evaluate the integral because the lower limit of the integral still needs evaluation; the top limit of the integral is $y_2 = x_D$ since the distillate product is made via a complete condensation of the vapor produced at the top of the column. However we will determine the value of y_1 for the top section latter as this is equal to the upper limit of the integral for the lower section of column.

The bottom section of the column is modeled with

$$y_{m+1} = \frac{\bar{L}}{\bar{V}} \left(x_m - x_B \right) \tag{3.26}$$

We will assume the feed is a saturated liquid since a liquid feed is most common, and the saturated liquid is simplest for the calculations involved. Based on balances around the feed point for these conditions

$$\bar{L} = L + F = RD + F \tag{3.27}$$

$$\bar{G} = G = L + D = D(R+1) \tag{3.28}$$

The recovery is defined as the fractional amount of solute in the feed which is recovered into the top product, and therefore

$$C_R = \frac{Dx_D}{Fx_F} \tag{3.29}$$

Thus

$$D = \frac{C_R x_F F}{x_D} \tag{3.30}$$

Thus

$$\bar{L} = \frac{RC_R F x_F}{x_D} + F \tag{3.31}$$

$$\bar{V} = \frac{C_R x_F F}{x_D}(R+1) \tag{3.32}$$

We will consider a feed flow rate equal to 1 mole/s as a basis (without loss of generality – scale-up does nothing to change the result of this calculation). Therefore

$$\bar{L} = \frac{RC_R x_F}{x_D} + 1 \tag{3.33}$$

$$\bar{V} = \frac{C_R x_F}{x_D}(R+1) \tag{3.34}$$

This produces the bottom section operating line

$$y_{m+1} = \frac{C_R x_F R + x_D}{C_R x_F (R+1)}\left(x_m - x_B\right) \tag{3.35}$$

This still has one value which is as yet unknown, the bottom product composition x_B. This can be calculated from the top product composition and product recovery. A component balance over the column gives

$$x_B B = F x_F - D x_D \tag{3.36}$$

Equation (17) relates the component recover to the feed and top product, such that

$$x_B B = F x_F - C_R x_F \tag{3.37}$$

Thus

$$x_B = \frac{F x_F - C_R x_F}{B} \tag{3.38}$$

And since the bottom product molar flow rate, *B*, is equal to the liquid molar flow rate in the bottom section of the column, it is given by equation (20). With some simplification, the bottom product is

$$x_B = \frac{x_F x_D (1 - C_R)}{C_R x_F R + x_D} \tag{3.39}$$

Thus

$$y_{m+1} = \frac{C_R x_F R + x_D}{C_R x_F (R+1)} \left(x_m - \frac{x_F x_D (1 - C_R)}{C_R x_F R + x_D} \right) \tag{3.40}$$

Using the definition of the number of transfer units applied to both sections of the column, we obtain

$$N_{OG} = \int_0^{y_{Int}} \frac{dy_{m+1}}{(y^* - y_{m+1})} + \int_{y_{Int}}^{x_D} \frac{dy_{n+1}}{(y^* - y_{n+1})} \tag{3.41}$$

The equations for y_{n+1} and y_{m+1} are the operating lines derived above, equations 3.17 and 3.40, and the function y^* is given for both sections by equation 3.23. The last variable required for the solution is the vapor phase mole fraction at the intersection between the two operating lines, y_{Int}. This can be found from the intercept between the *q*-line and the top-section operating line, equations 3.17 and 3.19, under the basis that $q = 1$, and $x_n = z_F = x_F$: since the feed is a liquid we can use the liquid phase mole fraction variable *x* rather than the more general *z*. This gives

$$y_{Int} = \frac{R x_F + x_D}{R + 1} \tag{3.42}$$

This fully parameterizes the two integrals in equation 3.41. We can calculate the driving force ($y - y^*$) for each section of the column by using the operating line to calculate x_n (for example) as a function of y_{n+1} and then using the x value in the equilibrium line to calculate the appropriate function for y^*. Rearranging equation 3.17 for x_n gives

$$x_n = \frac{y_{n+1}(R+1) - x_D}{R} \tag{3.43}$$

This can then be substituted into equation 3.23 to obtain the equilibrium vapor phase mole fraction.

We will integrate each of these independently, giving $N_{OG,T}$ for the top section, and $N_{OG,B}$ for the bottom section. To minimize the height of the packed column we need to minimize the sum of these two integrals.

The number of transfer units for the top section

$$N_{OG} = \int_{y_{In}t}^{y_i = x_D} \frac{1}{y^* - y_n} dy = \int_{y_{Int}}^{x_D} \frac{-(1-\alpha)\left(\frac{R+1}{R}\right)y_n + \left((1-\alpha)\frac{x_D}{R} + 1\right)}{(1-\alpha)\left(\frac{R+1}{R}\right)y_n^2 + \left(\alpha\left(\frac{R+1}{R}\right) - (1-\alpha)\left(\frac{x_D}{R}\right) - 1\right)y_n - \frac{\alpha x_D}{R}} dy_n$$

$$= \int_{y_{Int}}^{x_D} \frac{-C_{1n}y_n + C_{4n}}{C_{1n}y_n^2 + C_{2n}y_n + C_{3n}} dy_n \tag{3.44}$$

Where, $C_{1n} = (1-\alpha)\left(\frac{R+1}{R}\right)$

$$C_{2n} = \left(\alpha\left(\frac{R+1}{R}\right) - (1-\alpha)\frac{x_D}{R} - 1\right)$$

$$C_{3n} = -\frac{\alpha x_D}{R}$$

$$C_{4n} = (1-\alpha)\frac{x_D}{R} + 1$$

Using integral forms of

$$\int \frac{dx}{ax^2 + bx + c} = \frac{1}{\sqrt{b^2 - 4ac}} \ln\left(\frac{2ax + b - \sqrt{b^2 - 4ac}}{2ax + b + \sqrt{b^2 - 4ac}}\right) \tag{3.45}$$

$$\int \frac{xdx}{ax^2+bx+c} = \frac{1}{2a}\ln(ax^2+bx+c) - \frac{b}{2a\sqrt{b^2-4ac}}\ln\left(\frac{2ax+b-\sqrt{b^2-4ac}}{2ax+b+\sqrt{b^2-4ac}}\right) \quad (3.46)$$

Rearranging Eqs. 3.44 to

$$N_{OG,T} = \frac{-C_{1n}\int_{y_{Int}}^{x_D}\frac{y_n dy_n}{C_{1n}y_n^2+C_{2n}y_n+C_{.3n}} + C_{4n}\int_{y_{Int}}^{x_D}\frac{1dy_n}{C_{1n}y_n^2+C_{2n}y_n+C_{3n}}}{} \quad (3.47)$$

Solving Eqs. (3.47), we get the result

$$N_{OG,T} = \left[\frac{C_{4n}}{\sqrt{C_{2n}^2-4C_{1n}C_{3n}}}\ln\left(\frac{2C_{1n}y_n+C_{2n}-\sqrt{C_{2n}^2-4C_{1n}C_{3n}}}{2C_{1n}y_n+C_{2n}+\sqrt{C_{2n}^2-4C_{1n}C_{3n}}}\right) + \frac{C_{1n}C_{2n}}{2C_{1n}C_{2n}\sqrt{C_{2n}^2-4C_{1n}C_{3n}}}\times \ln\left(\frac{2C_{1n}y_n+C_{2n}-\sqrt{C_{2n}^2-4C_{1n}C_{3n}}}{2C_{1n}y_n+C_{2n}+\sqrt{C_{2n}^2-4C_{1n}C_{3n}}}\right) - \frac{C_{1n}}{2C_{1n}}\ln\left(C_{1n}y_n^2+C_{2n}y_n+C_{3n}\right)\right]_{y_{Int}}^{x_D} \quad (3.48)$$

Rearranging to

$$N_{OG,T} = \left[\frac{C_{1n}+\frac{C_{2n}}{2}}{\sqrt{C_{2n}^2-4C_{1n}C_{3n}}}\ln\left(\frac{2C_{1n}y_n+C_{2n}-\sqrt{C_{2n}^2-4C_{1n}C_{3n}}}{2C_{1n}y_n+C_{2n}+\sqrt{C_{2n}^2-4C_{1n}C_{3n}}}\right) - \frac{1}{2}\ln\left(C_{1n}y_n^2+C_{2n}y_n+C_{3n}\right)\right]_{y_{Int}}^{x_D} \quad (3.49)$$

Take lower limit ($y_{Int} = \frac{Rx_F + x_D}{R+1}$) and upper limit (x_D) and rearrange term of this, the solution become to:

$$N_{OG,T} = \frac{C_{4n}+\frac{C_{2n}}{2}}{\sqrt{C_{2n}^2-4C_{1n}C_{3n}}}\ln\left[\frac{\left(2C_{1n}x_D+C_{2n}-\sqrt{C_{2n}^2-4C_{1n}C_{3n}}\right)\left(2C_{1n}y_{Int}+C_{2n}+\sqrt{C_{2n}^2-4C_{1n}C_{3n}}\right)}{\left(2C_{1n}x_D+C_{2n}+\sqrt{C_{2n}^2-4C_{1n}C_{3n}}\right)\left(2C_{1n}y_{Int}+C_{2n}-\sqrt{C_{2n}^2-4C_{1n}C_{3n}}\right)}\right] - \frac{1}{2}\ln\left[\frac{C_{1n}x_D^2+C_{2n}x_D+C_{3n}}{C_{1n}y_{Int}^2+C_{2n}y_{Int}+C_{3n}}\right] \quad (3.50)$$

$$N_{OG,B} = \int_0^{y_{Int}} \frac{1}{y^* - y_m} dy_m \tag{3.51}$$

Solving Equation 3.18 for x_m:

$$x_m = y_m \left[\frac{x_F \times CR \times (R+1)}{x_F \times CR \times R + x_D} \right] + x_W \tag{3.52}$$

Rewriting Eqs. 3.21 to

$$y^* = \frac{\alpha x_m}{1 - x_m(1-\alpha)} \tag{3.53}$$

Then, after substituting into the integral for the bottom section and rearranging, we get

$$N_{OG,B} = \int_0^{y_{Int}} \frac{y_m + \left(\frac{x_F \times CR \times R + x_D}{x_F \times CR \times (R+1)} \right) \left(\frac{1}{1-\alpha} \right) \left(x_W (1-\alpha) - 1 \right)}{-y_m^2 + \frac{1 - x_W + \alpha x_W - \alpha \left(\frac{x_F \times CR \times (R+1)}{x_F \times CR \times R + x_D} \right)}{(1-\alpha)\left(\frac{x_F \times CR \times (R+1)}{x_F \times CR \times R + x_D} \right)} y_m - \alpha x_W \left(\frac{x_F \times CR \times R + x_D}{x_F \times CR \times (R+1)} \right) \left(\frac{1}{1-\alpha} \right)} dy_m \tag{3.54}$$

or

$$-N_{OG,B} = \int_0^{y_{Int}} \frac{y_m + \left(\frac{x_F \times CR \times R + x_D}{x_F \times CR \times (R+1)} \right) \left(\frac{1}{1-\alpha} \right) \left[x_W (1-\alpha) - 1 \right]}{y_m^2 - \frac{1 - x_W + \alpha x_W - \alpha \left(\frac{x_F \times CR \times (R+1)}{x_F \times CR \times R + x_D} \right)}{(1-\alpha)\left(\frac{x_F \times CR \times (R+1)}{x_F \times CR \times R + x_D} \right)} y_m + \alpha x_W \left(\frac{x_F \times CR \times R + x_D}{x_F \times CR \times (R+1)} \right) \left(\frac{1}{1-\alpha} \right)} dy_m \tag{3.55}$$

$$-N_{OG,B} = \int_0^{y_{Int}} \frac{y_m + C_{3m}}{y_m^2 + C_{1m} y_m + C_{2m}} dy_m \tag{3.56}$$

Where,
$$C_{1m} = -\left(\frac{x_F \times CR \times R + x_D}{x_F \times CR \times (R+1)}\right)\left(\frac{1}{1-\alpha}\right)\left[1 - x_W + \alpha x_W - \alpha \frac{x_F \times CR \times (R+1)}{x_F \times CR \times R + x_D}\right]$$

$$C_{2m} = \left(\frac{\alpha x_W}{1-\alpha}\right)\left(\frac{x_F \times CR \times R + x_D}{x_F \times CR \times (R+1)}\right)$$

$$C_{3m} = \left(\frac{x_F \times CR \times R + x_D}{x_F \times CR \times (R+1)}\right)\left(\frac{1}{1-\alpha}\right)\left[x_W(1-\alpha) - 1\right]$$

Rearranging Eq. 3.56 to

$$-N_{OG,B} = \int_0^{y_{Int}} \frac{y_m}{y_m^2 + C_{1m} y_m + C_{2m}} dy_m + C_{3m} \int_0^{y_{Int}} \frac{1}{y_m^2 + C_{1m} y_m + C_{2m}} dy_m \quad (3.57)$$

Solving 3.57 we get the result

$$-N_{OG,B} = \left[\frac{1}{2}\ln\left(y_m^2 + C_{1m} y + C_{2m}\right) - \frac{C_{1m}}{2\sqrt{C_{1m}^2 - 4C_{2m}}}\ln\left(\frac{2y_m + C_{1m} - \sqrt{C_{1m}^2 - 4C_{2m}}}{2y_m + C_{1m} + \sqrt{C_{1m}^2 - 4C_{2m}}}\right)\right.$$
$$\left. + \frac{C_{3m}}{\sqrt{C_{1m}^2 - 4C_{2m}}}\ln\left(\frac{2y_m + C_{1m} - \sqrt{C_{1m}^2 - 4C_{2m}}}{2y_m + C_{1m} + \sqrt{C_{1m}^2 - 4C_{2m}}}\right)\right]_0^{y_{Int}} \quad (3.58)$$

Rearranging to

$$-N_{OG,B} = \left[\frac{C_{3m} - \frac{C_{1m}}{2}}{\sqrt{C_{1m}^2 - 4C_{2m}}}\ln\left(\frac{2y_m + C_{1m} - \sqrt{C_{1m}^2 - 4C_{2m}}}{2y_m + C_{1m} + \sqrt{C_{1m}^2 - 4C_{2m}}}\right) + \frac{1}{2}\ln\left(y_m^2 + C_{1m} y_m + C_{2m}\right)\right]_0^{y_{Int}} \quad (3.59)$$

Take lower limit (zero) and upper limit ($y_{Int} = \frac{Rx_F + x_D}{R+1}$) and rearrange term of this, the solution become to:

$$-N_{OG,B} = \frac{C_{3m} - \frac{C_{1m}}{2}}{\sqrt{C_{1m}^2 - 4C_{2m}}} \ln\left[\frac{\left(2y_{Int} + C_{1m} - \sqrt{C_{1m}^2 - 4C_{2m}}\right)\left(C_{1m} + \sqrt{C_{1m}^2 - 4C_{2m}}\right)}{\left(2y_{Int} + C_{1m} + \sqrt{C_{1m}^2 - 4C_{2m}}\right)\left(C_{1m} - \sqrt{C_{1m}^2 - 4C_{2m}}\right)}\right] + \frac{1}{2}\ln\left[\frac{y_{Int}^2 + C_{1m}y_{Int} + C_{2m}}{C_{2m}}\right] \quad (3.60)$$

or

$$N_{OG,B} = -\frac{C_{3m} - \frac{C_{1m}}{2}}{\sqrt{C_{1m}^2 - 4C_{2m}}} \ln\left[\frac{\left(2y_{Int} + C_{1m} - \sqrt{C_{1m}^2 - 4C_{2m}}\right)\left(C_{1m} + \sqrt{C_{1m}^2 - 4C_{2m}}\right)}{\left(2y_{Int} + C_{1m} + \sqrt{C_{1m}^2 - 4C_{2m}}\right)\left(C_{1m} - \sqrt{C_{1m}^2 - 4C_{2m}}\right)}\right] - \frac{1}{2}\ln\left[\frac{y_{Int}^2 + C_{1m}y_{Int} + C_{2m}}{C_{2m}}\right] \quad (3.61)$$

3.2.1 The Total Number of Transfer Units (N_{OG}):

The total number of transfer units necessary in the column is simply the sum of the numbers of transfer units in both sections:

$$N_{OG} = N_{OG,T} + N_{OG,B} \quad (3.62)$$

This equation (the sum of $N_{OG,T}$ and $N_{OG,B}$) is a relatively simple function of the reflux ratio *R*, as it appears in the constants of these two terms. Thus, the function can be differentiated with respect to *R*, and finding the value of *R* which results in the differential being equal to zero gives the value of *R* that will result in the minimum number of transfer units for the entire column, and will also be a close approximation to the value *R* for the minimum number of theoretical stages. The analytical differential of the function can be found without trouble in programs such as Mathematica or Reduce. It is however too long to show here, taking up in excess of 10 printed pages in Mathematica format! Unfortunately the equation is too extensive for Mathematica or Reduce to find a suitable simplification (the computer runs out of memory before a solution is found, if such a reduction exists). In addition the programs cannot find an analytical solution to the derivative being equal to zero. We are still working on this problem to find simplifications

or analytical solutions. However, we are able to solve the equation numerically for suitable values of the parameters used in the method. These results are shown in chapter V.

A similar method was used to obtain a solution for the case of a saturated vapor feed. In this case the q-line for the feed is a different function, and hence the operating lines and the intersection of the operating lines is different. However the derivation is similar, and not difficult to construct based on the work presented above.

Chapter IV

Results and Discussion for the Solution Mediated Transformation

4.1 Simulations Within and Outside the Metastable Zone

Simulation results using the parameters for crystal growth rate kinetics, crystal nucleation rate kinetics, crystal dissolution rate kinetics, and induction time data from previous research from the group [10-12] on the species' α-DL-methionine and γ-DL-methionine were compared to experimentally measured SMT data for DL-methionine. Although the simulation can predict a large number of variables as a function of experiment time (relating to the particle size distributions of the two polymorphs, the total mass and volume of crystals in both polymorphic forms, the total concentration of DL-methionine remaining in the solution, the mass fraction of DL-methionine in a particular polymorphic form, among others) the main variables we are interested in and would measure during a SMT are the concentration of the solute in solution as a function of time and the mass fraction of the crystal in a particular polymorphic form.

Two sets of simulations were performed. The first set had no fitted parameters; all parameter values in the model were given based on models with concentration driving forces that were predicted on measurements of the underlying physical phenomena (equilibrium between solid and liquid phases, crystal nucleation, crystal growth, and crystal nucleation) for the two polymorphs published in our previous articles. The results for these simulations are shown in Figure 4.1a for a batch crystallization where the initial concentration of solute is outside the secondary nucleation threshold of the stable polymorph (causing an instantaneous nucleation of the stable polymorph), and Figure 4.2a where the initial concentration of solute is within the secondary nucleation threshold of the stable polymorph (causing an delayed nucleation of the stable polymorph). It can be seen that this model greatly over-predicts the rate of the conversion of α-DL-methionine to γ-DL-methionine. In the case of the experiment outside the secondary nucleation threshold (having spontaneous nucleation) the conversion being complete in the model prediction within *circa* 500 min whereas in the experiments full conversion requires approximately 5000 min. In the case of the experiment within the secondary nucleation threshold the experiment reaches complete conversion only after 12000 min whereas the model predicted complete conversion within 6000 min.

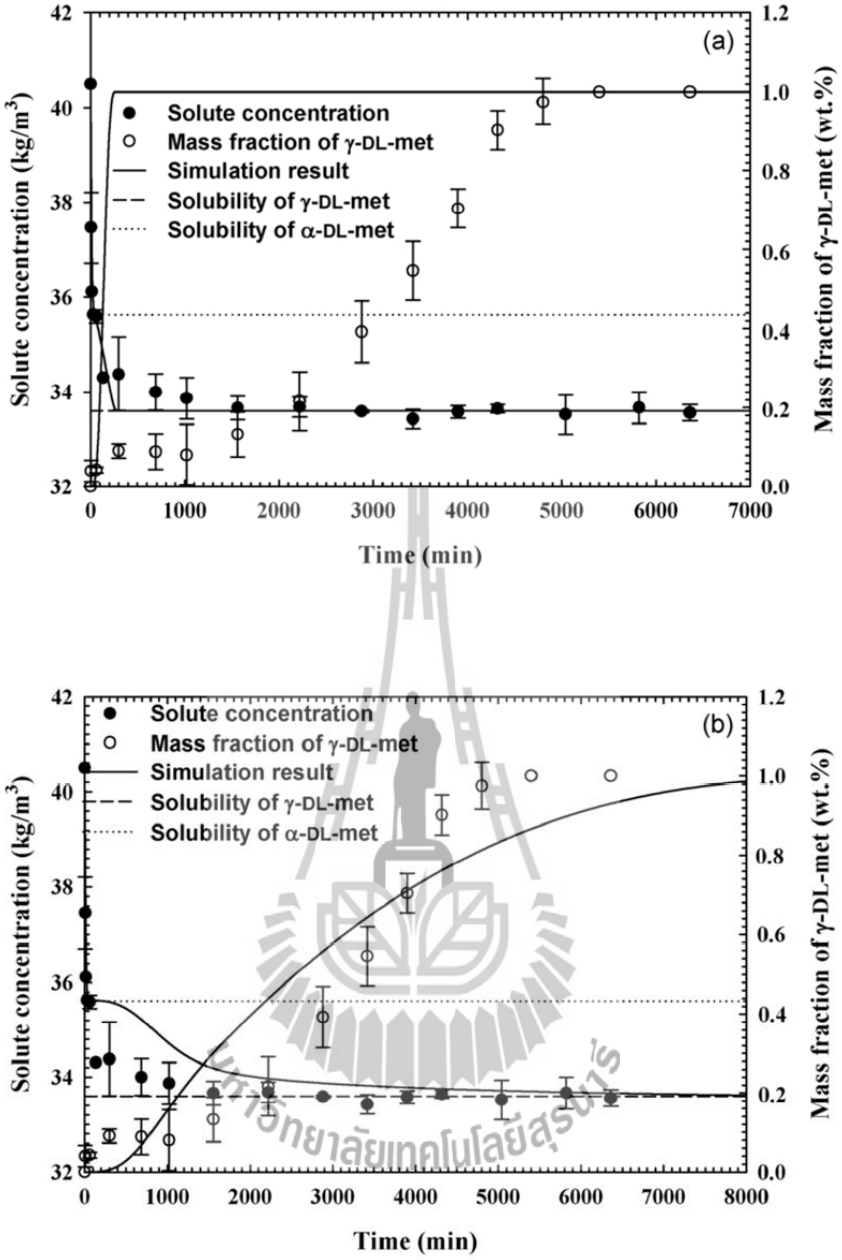

Fig. 4.1 Solute concentration and fraction of γ-DL-met in the crystal phase during the polymorphic transformation for C_0 = 40.5 kg m^{-3}: (a) the dissolution kinetics obtained from a previous work [11], (b) the dissolution kinetics were estimated from the combination of the modeling method with the SMT experimental data.

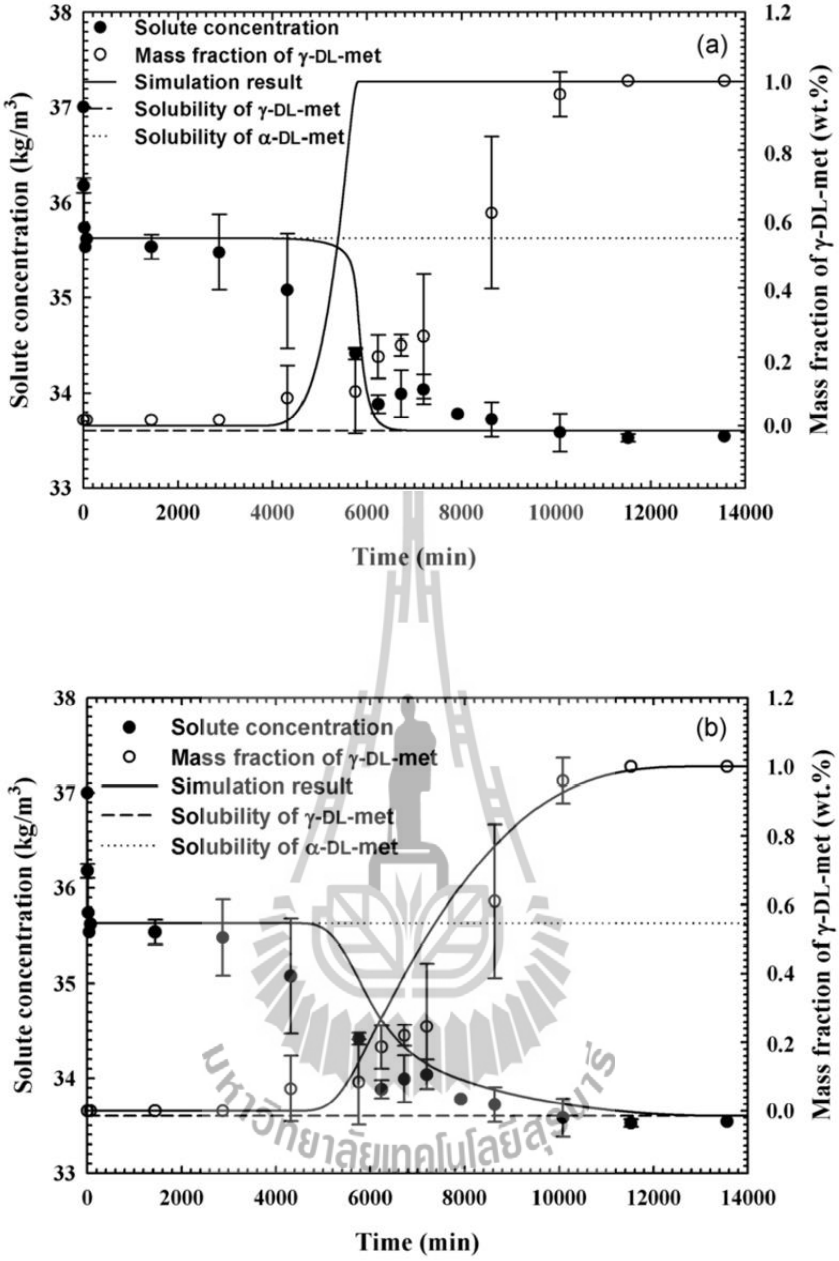

Fig. 4.2 Solute concentration and fraction of γ-DL-met in the crystal phase during the polymorphic transformation for C_0 = 37.0 kg m^{-3}: (a) the dissolution kinetics obtained from a previous work [11], (b) the dissolution kinetics were estimated from the combination of the modeling method with the SMT experimental data.

Analysis of the model in comparison with the experimental results shows that the rate of conversion between the two polymorphs is controlled by three mechanisms, the rate

of dissolution of the unstable polymorph, the rate of nucleation of the stable polymorph, and the rate of crystal growth of the stable polymorph.

More detailed descriptions of one of the *a priori* modeling of one of these experiments is shown in Figure 4.3 (solute concentration) and Figure 4.4 (stable polymorph fraction). Note that the population balance model is completely independent of the experimental SMT results since it uses fundamental models of growth, dissolution, and nucleation parameterized on experimental measurements of the mechanisms in isolation.

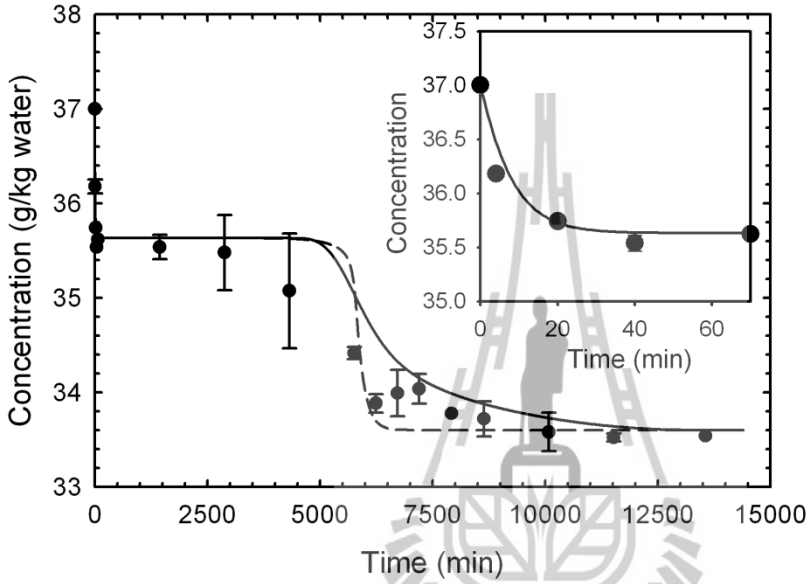

Fig. 4.3 The concentration of DL-methionine as a function of time during SMT of α-DL-methionine to γ-DL-methionine starting at a concentration within the instantaneous Secondary Nucleation Threshold (SNT) of γ-DL-methionine. The first 70 min of the transformation are expanded to highlight the crystal growth of the metastable form. Experimental data ● ; prediction of *a priori* population balance model – – – ; prediction of population balance model with a fitted dissolution rate constant —— .

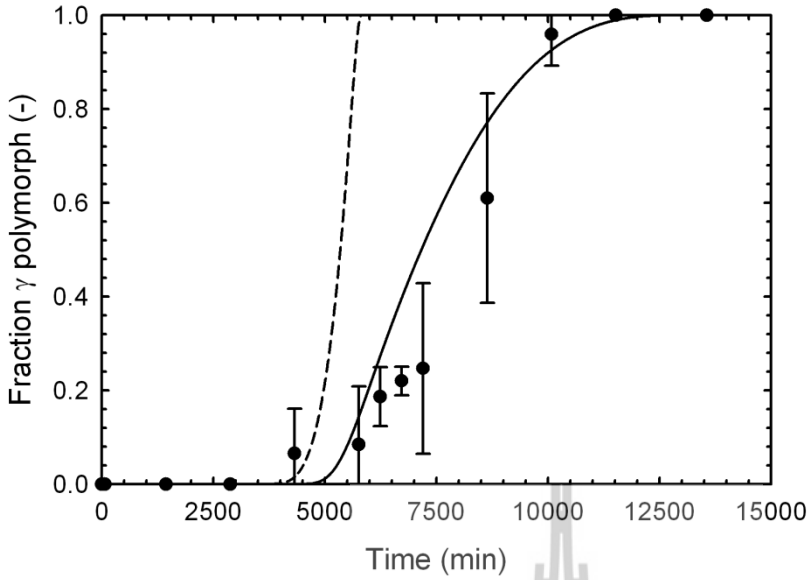

Fig. 4.4 The fraction of DL-methionine in the γ-DL-methionine form as a function of time during SMT of α-DL-methionine to γ-DL-methionine starting at a concentration within the instantaneous SNT of γ-DL-methionine. Experimental data ● ; prediction of *a priori* population balance model – – – ; prediction of population balance model with a fitted dissolution rate constant —— .

It is clear that the predictions of the *a priori* model are not good. Although the concentration data is fitted acceptably, the polymorph fraction results are not fitted at all well. The predicted polymorph fractions for the stable polymorph increase far too rapidly compared to the experimental results, showing that one of the rates in this step is much faster in the model than it is in the experiments. Analysis of the data showed that the mechanism that was not fitted well was the dissolution rate of the metastable polymorph. The dissolution kinetics is assumed to be first order and therefore only have a single parameter, the dissolution rate constant. This parameter was allowed to vary in order to fit the experimental data for these experiments (and also experimental data performed above the SMT), and the results are shown using the solid line in Figures 4.3 and 4.4. The second set of predictions on Figure 4.3 and 4.4 shows very good agreement with the experimental data, and use of the same rate constant in other SMT data (for instance data outside of the instantaneous SNT) also showed a very good fit. However in achieving this improved result the dissolution rate constant decreased from the measured value of 5.8×10^{-7} m/s to a value of 7.5×10^{-9} m/s, a quite drastic re-evaluation of this constant! The error in the initial

value may be due to an assumption that the dissolution rate of both polymorphs is mass transfer controlled, and that therefore the dissolution rate of the two polymorphs should be equal for an equal driving force, considering that the two polymorphs have different solubility and therefore a different driving force at an equal concentration. The metastable polymorph was found to occur as very small crystals of irregular shape since it can only be produced from precipitation of the species from acidic solutions. Therefore the dissolution rate measurements were performed on the stable polymorph and the dissolution model transformed across to the metastable polymorph. Although this appears incorrect in this instance it is a commonly used assumption. For instance the Sherwood correlation for mass transfer is commonly used to predict dissolution rate constants of a metastable polymorph [8,13], which indicates an assumption that the mass transfer is rate controlling for dissolution. Even when allowing a single parameter to float results in a good fit to the data, it is not clear whether the model parameters are now an accurate representation of the real mechanisms. The change between the measured dissolution kinetics and the predicted kinetics is larger than could be expected, with the fitted dissolution rate constant being almost two orders of magnitude smaller than the experimental one for the stable polymorph.

Similar results were seen in experiments starting outside of the instantaneous SNT. When the fully *a priori* model was used the agreement between the model predictions and the experimentally measured SMT were poor, particularly during the step involving the dissolution of α-DL-methionine and the growth of γ-DL-methionine. Using the same fitted dissolution rate constant as with the first set of experiments allowed a very good fit to the experimental data. The following section discusses particular improvements to understanding and modeling the underlying mechanisms involved in the SMT which could assist in achieving accurate *a priori* modeling of the SMT.

4.1.1 Improvements Required to Obtain Accurate SMT Models

The modeling of the underlying phenomena for the SMT tend to be very simple engineering models of the phenomena (for instance the use of power law models to represent the relationship between *average* kinetics for a phenomenon and driving forces) that do not fully represent the complexity of what occurs in real systems. The researchers in this project completed a survey of prior experimental work to determine in what ways models of the underlying phenomena, such as nucleation, growth, and dissolution kinetic

equations could be improved so that complete models of SMT could better represent real data. Discussion of why these models may fail to accurately model the systems studied and what further understanding relating to these processes is required is discussed in this section. An illustration of the complexity of crystal growth and dissolution kinetics is shown in Figure 4.5, which shows artificial data which could describe a typical system. The plot is based on similar data for step velocities in potassium bichromate [14] and crystal growth and dissolution rates for sucrose [15]. This plot will help to illustrate many of the points discussed below.

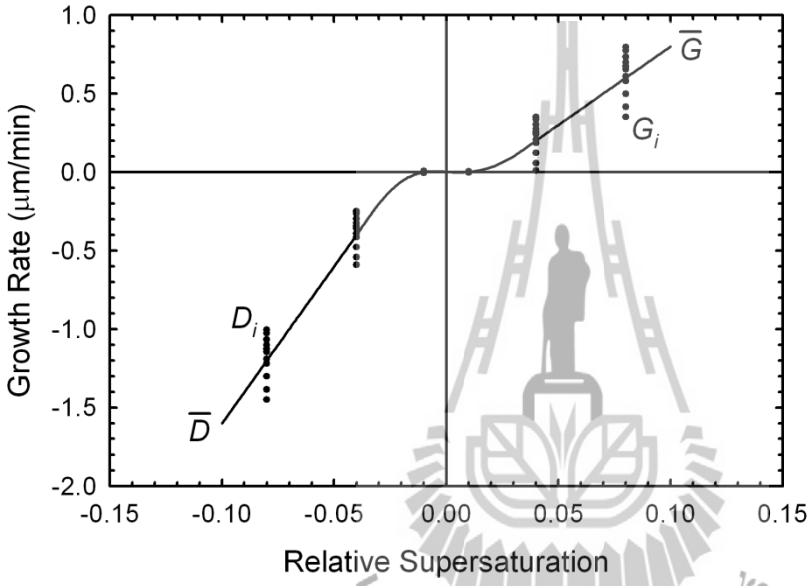

Fig. 4.5 Illustrative data for crystal growth rates and dissolution rates as a function of relative supersaturation. In carefully measured experimental data, growth rate dispersion, dissolution rate dispersion, a null supersaturation, and a null undersaturation are all evident.

4.1.2 The Growth Rate Model & Null Supersaturation

Carefully measured experimental data on crystal growth rates at low values of the supersaturation typically find a region above the solubility where crystal growth does not occur (see the region $0 < \sigma < 0.01$ on Figure 4.5). This region has an upper bound called the null supersaturation, below which crystal growth is negligible or zero. For instance Khaddour *et al.* [16] have commented that for sucrose "… obtained growth rate curves show a practical stoppage of the growth process at $\sigma \approx 0.04$" and comment that this phenomenon agrees with measurements taken over 40 years previously [17]. The

phenomenon has also been observed by a range of groups in pure and impure solutions [18-21]. Neglecting the null supersaturation will result in a model that does not predict the crystallization kinetics near the solubility of either polymorph very well.

A second problem with crystal growth rate kinetics is that the relative significance of the rate of mass transfer and the rate of surface integration is often not taken into account. There are two methods that can be used to correctly account for this; the crystal growth rates can be measured in an agitated vessel similar to the crystallizer used for SMT over a range of agitation rates, and the role of mass transfer predicted from these experiments, or the crystal growth rates can be measured under surface integration controlled conditions and the mass transfer kinetics predicted from mass transfer correlations. It is important to take this into account in the model, since the relative significance of the rate of mass transfer might be significantly different in the crystallization vessel compared to the solution in which the experiments to determine the crystal growth rates were performed.

4.1.3 Dissolution Rate Model and Null Undersaturation

The dissolution rate modeling typically contains the same difficulties as the crystal growth rate modeling. In the case of SMT modeling, the null undersaturation (the region $-0.01 < \sigma < 0$ on Figure 4.5) is a more significant feature than the null supersaturation. This is because the system may spend a considerable time at, or very close to, the supersaturation of the metastable polymorph, which is α-DL-methionine in the system discussed in the section above. At the start of the SMT the system may maintain a concentration close to the solubility of the metastable polymorph while this polymorph dissolves, depending on the relative kinetics of the crystal growth of the stable polymorph and the dissolution kinetics of the metastable polymorph. During this period the dissolution rate of the metastable polymorph may be very low (due to the null undersaturation) compared with the rate predicted based on a model parameterized by dissolution measurements at higher undersaturation values. This slowing of the dissolution of the metastable polymorph may greatly reduce the rate of the SMT, and this is likely what has occurred in the case study above.

A second consideration is whether the dissolution rate of a crystal is really mass transfer controlled for the species under consideration. If the dissolution rate is not fully mass transfer controlled then the relative rates of the surface reaction and mass transfer need to be investigated under conditions similar to those under which the SMT takes place.

It is possible that for a large number of species the assumption that dissolution may be modeled using mass transfer correlations may be inadequate.

4.1.4 Growth Rate Dispersion (GRD) and Dissolution Rate Dispersion (DRD)

Careful measurements of crystal growth rates using a large population of crystals show that there is significant crystal growth rate dispersion for crystals grown under the same conditions of growth. A typical example is a recent study by Srisa-nga *et al*., [22] which showed that the fastest five percent of a population of α-glucose monohydrate crystals had growth rates that were six to eight times larger than the slowest five percent of the population. This is shown in Figure 3 by comparison of the data G_i to the mean value as a function of supersaturation, $\bar{G}$. This is important since the population balance models for the polymorphs require a mass balance closure in order to correctly predict the time dependent supersaturations of all relevant polymorphs. This can only be achieved accurately if a full growth rate distribution (or dissolution rate distribution) is known such that the time dependent crystal size distributions are modeled accurately. If the time dependence of the supersaturation is not modeled adequately then the rates of the significant mechanisms (growth, dissolution, nucleation, induction time, etc…) will also be incorrect.

Currently available growth rate models only attempt to model the mean crystal growth rate of a distribution, and such a form is typically used in the population balance models without attempting to account for GRD. Using only a mean crystal growth rate when GRD is significant miscalculates the mass balance by a significant amount. As an example of the significance of GRD to the mass balance, consider a population of 1×10^6 crystals which are a monosize distribution at 40 μm, and are cubic in habit. These crystals grow for a period of 1 h with a growth rate distribution which is normally distributed with a mean growth rate of 1 μm/min and a standard deviation of 0.38 μm/min (which equates to the fastest five percent of crystals growing at 7.3 times the rate of the slowest five percent). The end result of this growth is a population of crystals with a normally distributed crystal size distribution that has a mean of 100 μm and a standard deviation of 22.8 μm. The volume of these product crystals is 1.156 mL, whereas if only the mean growth rate was used the volume predicted for the product would be exactly 1 mL. Thus, use of only the mean growth rate has underestimated the volume by fifteen percent (and the change in volume due to growth by a larger amount). It is important to note that even if the growth

rate distribution is symmetric the reduction in volume produced caused by the slow growing crystals is *not sufficient* to cancel the increase in volume produced due to the fast growing crystals. Accurate mass balances require that the population balance accounts for the crystal growth rate dispersion if it is significant, and nearly all carefully measured crystal growth rate data has observed significant GRD. If the mass balance calculation used with the population balance is not sufficiently accurate then the supersaturation dependent parameters in the model will also be incorrect, leading to a poor prediction.

Similar arguments can be made for the effect of DRD. This is a less well known phenomenon than GRD, however it is known to exist [14,15]. Dissolution of the metastable polymorph is an extremely significant part of the SMT, and thus DRD needs to be accurately modeled in the population balance if it exists to a significant extent in the system.

4.1.5 Nucleation Rate Modeling

There is very incomplete knowledge about nucleation in systems containing two or more polymorphs. In particular it is usually assumed that secondary nucleation only occurs with the aid of parent crystals of the same form of crystal as that which is nucleating. This has been shown to not be true in previous studies. For instance Elankovan and Berglund [23] have shown via Raman spectroscopy that secondary (contact) nuclei of both anhydrous α-glucose and α-glucose monohydrate can form from parent crystals of anhydrous α-glucose. The authors used the result to suggest that contact nucleation is due to the removal of a semiordered absorbed layer from the surface of the parent crystal, and that this partly disordered cluster is able to reform into a different structure than the parent crystal it is removed from. Although these two forms are not polymorphs (but an anhydrous form and its monohydrate) the result that the material removed from the parent is both disordered and able to rearrange into a different form has important implications in the study of solution mediated transformation. This makes the mechanism of nucleation of the stable polymorph in suspensions containing crystals of the metastable polymorph difficult to model. The rate is likely to be somewhere between the primary nucleation rate (nucleation from a solution containing none of the polymorphs or hydrates/solvates of the solute) and the secondary nucleation rate where secondary nuclei are produced from the correct (stable) polymorph. At the moment there appears to be no way to fundamentally model this. Experiments for secondary nucleation can be performed in similar systems

(attempting to nucleate the stable polymorph from suspensions containing the metastable polymorph) however in such a case it is difficult to prove whether the initial nuclei formed are the stable polymorph, the metastable polymorph, or a mechanical mixture of the two polymorphs.

A further consideration in modeling nucleation rates is that the rate of secondary nucleation will depend strongly on the agitation in the system, the fluid dynamics, and also the suspension density. Thus, nucleation rates should be measured in a system with similar properties to that likely to be used for the SMT, if possible.

Another very significant problem in the measurement of nucleation kinetics in systems containing more than one polymorph is to distinguish the nucleation of the two polymorphs under conditions where two or more polymorphs may nucleate simultaneously. This is in principle a very difficult task, however there have been two approaches used in the literature. The first method is to use spectroscopic and/or particle characterization methods to characterize the polymorphic form of the nuclei. An example of the use of this method is work by Schöll *et al*. [24], who measured nucleation rates in the polymorphic system of L-glutamic acid, determining the form of the crystal with in-situ Raman spectroscopy and by a Particle Vision and Measurement (PVM) system. The PVM system can be useful when the polymorphs have strongly differing habits, as in the case of α- and β- L-glutamic acid. This method is likely to produce accurate results, although care needs to be taken that there is no phase transformation occurring before a definite determination can be made, for example before the spectroscopic signal is strong enough and/or before the particles are large enough to be detected or large enough to maintain a characteristic shape. The second method that has been used is to search for a discontinuity in the nucleation kinetics that could be attributed to a change in the nucleating species, as has been demonstrated by Teychené and Biscans [25] in a study of nucleation of the polymorphs of eflucimibe. In this method care needs to be taken to ensure that the discontinuity is not due to a change in the nucleation mechanism of a single polymorph, from a heterogeneous to a homogeneous mechanism for example. Further fundamental studies concerning nucleation in polymorphic systems are certainly warranted.

4.1.6 Induction Time Prediction

The induction time *may* be independent of the nucleation rate, however many of the difficulties discussed in section 3.4 will also be apparent in attempting to model the

induction time of the stable polymorph. Induction times are either measured in terms of metastable zone width (MSW) values or nucleation thresholds (NT); however the induction time is strongly dependent on the range of conditions that the solution experiences between the formation of the solution and the nucleation event (or the detection of nucleation) and these two methods will give different induction times for the same nucleation condition. Thus, the induction time is extremely difficult to predict using a fundamental model, and is instead typically fitted with empirical relationships. In either case a decision is needed as to whether the primary nucleation threshold or the secondary nucleation threshold is most applicable to the system being modeled, but the presence of the metastable polymorph makes this decision difficult. It is likely that the nucleation threshold is somewhere between the primary nucleation threshold and the secondary nucleation threshold, perhaps closer to the latter.

A second difficulty with induction time measurements is their wide scatter; replicate induction time measurements can often vary by hours, so a large number of replicates are needed to accurately describe the induction time. Even when this is done, the induction time for a particular SMT experiment may be anywhere within the distribution of induction times predicted by the experimental induction times at a particular condition. Induction times for secondary nucleation also suffer from the fact that the induction time tends to depend on the amount and size of the parent crystals used to induce the secondary nucleation, and the agitation and fluid dynamics that is present in the system. Induction time experiments for secondary nuclei need to be made in a system as close as possible to the system in which the SMT takes place.

In some models for the induction time (or nucleation threshold or metastable zone width) the phenomenon is seen as an artificial construct caused only by the fact that nuclei formed as soon as the solution is produced still require a certain period of time to obtain a large enough number concentration and size in the solution to be able to be detected. In this case we need to ask whether a model of the phenomenon is required at all? The phenomenon should be able to be accounted for within the nucleation and growth rate models, without the need for an additional condition on the population balance. If the modeling is done in this way care needs to be taken to account for the fact that the crystals that have a size between the size of a critical nucleus and the size of a detectable crystal will have lower growth rates than the detectable crystals, due to the size dependence of the solubility for very small crystals. More recently there has been some discussion as to

whether some part of the metastable zone is, in fact, a true metastable state [26]. Further studies on the phenomenon are necessary to clarify this issue.

4.1.7 The Effect of Changes in Shape

As mentioned earlier, closure of the population balance models requires a mass balance to determine the supersaturations of all relevant polymorphs as a function of time. This is necessary in order to accurately determine the kinetics as a function of time. The mass balance should be calculated from either the second or third moments of the crystal size distribution of each polymorph, and the relevant shape factors. Typically in the population balance models it is assumed that the shape factors are constant with respect to time, however in certain cases this assumption may be violated. In particular it is known that particular facial growth rates of certain crystals have a significant dependence on the level of supersaturation, and that therefore the aspect ratios and the shape factor of the crystals will change during the SMT. A similar effect may occur during the dissolution of the metastable phases. In most cases this effect is likely to be minor, although it is necessary to consider the possibility if accurate models of the other phenomenon still fail to adequately describe the SMT.

4.1.8 Effect of Crystalline Perfection on Rates and Solubility

Most kinetic data (in particular for growth and dissolution measurements) is measured based on large, very perfect seed crystals. In addition, most nucleation rate data is performed at low enough supersaturation that well-formed crystals are created. The metastable form in SMT may not be in agreement with these measurements: often the initial metastable phase is irregular and imperfect in shape and quality, and may consist of very small sized particles. Strongly imperfect crystals and also very small crystals have different solubility, and different kinetics when the change in solubility is taken into account, than large near perfect crystals. This may lead to incorrect estimates from all the parameter models (the growth rate model, the dissolution rate model, the nucleation rate model, and the induction time model) for the metastable polymorph in particular, based on measurements in more ideal systems.

Chapter V

Results and Discussion for the Open Steam Distillation

As mentioned, although it has been shown to be possible to find the function relating all variables to the number of transfer units (a more convenient task than evaluating the number of stages) and also to take the derivative of this equation with respect to the reflux ratio (and therefore to set this derivative equal to zero to define the reflux ration at which the number of stages should be a minimum) it has not been possible to solve this equation analytically to give an exact answer for any conditions (see chapter 3 on the mathematical model for details of the derivation and equations involved). It has been possible to solve the equation numerically for any given set of conditions however. Some examples are shown below.

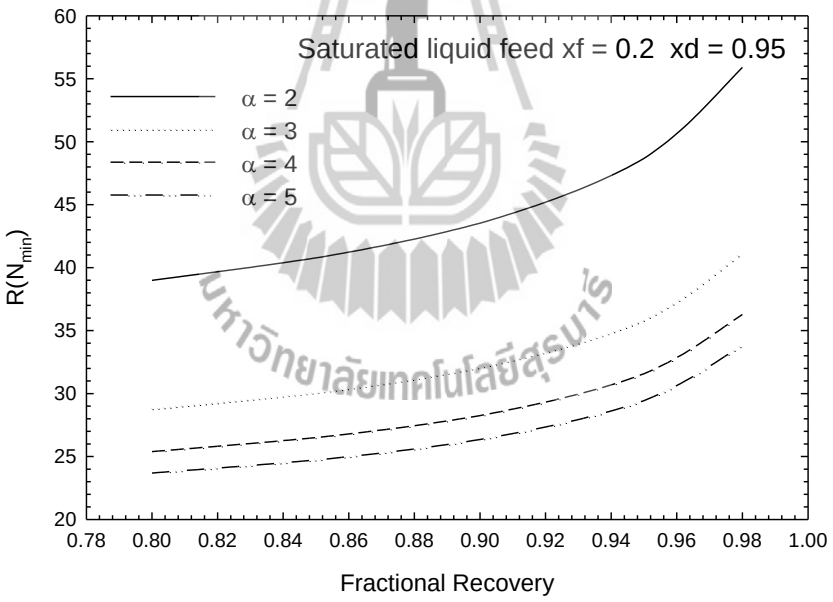

Fig. 5.1 Reflux ratio necessary for the minimum number of stages in an open steam distillation column with a saturated liquid feed with solute mole fraction of 0.2. The top product composition is 0.95, and % recovery and relatively volatility as given in the figure.

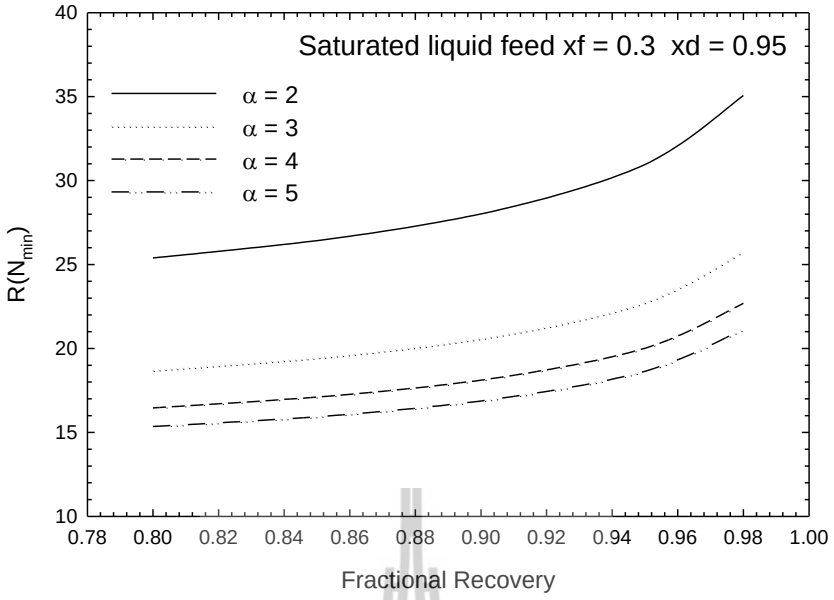

Fig. 5.2 Reflux ratio necessary for the minimum number of stages in an open steam distillation column with a saturated liquid feed with solute mole fraction of 0.3. The top product composition is 0.95, and % recovery and relatively volatility as given in the figure.

The examples given are plotted between 80% recovery and 98% recovery; this is the likely range in industrial practice since smaller recoveries are uneconomic because the loss (greater than 20%) of product is too significant, and recoveries greater than 98% will be uneconomic because of the requirement for a very large number of stages, or larger reflux ratios. The trends of the results are in agreement with expectations, in that an increase in % recovery increases the reflux ratio necessary to achieve a minimum number of stages for open steam distillation, as does a decrease in the relative volatility of the binary mixture. The effect of the feed composition was not forecasted, however clearly a decrease in the amount of solute in the feed greatly affects the ability to easily recover this solute, thus leading to an increase in the reflux ratio required to give the minimum number of stages. Note that these conclusions are *only* correct for open steam distillation columns; the reflux ratio required for a minimum number of stages for a column with a reboiler is a reflux ratio of infinity (as is well known).

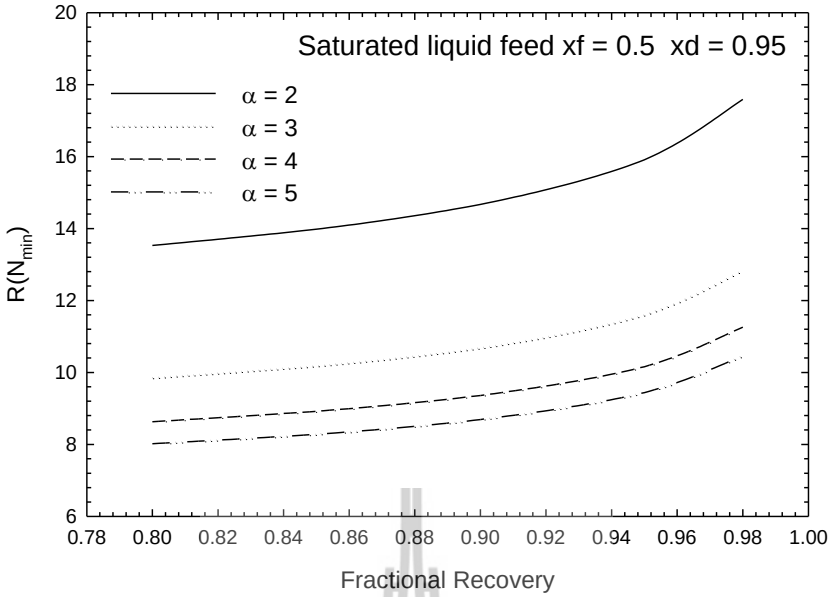

Fig. 5.3 Reflux ratio necessary for the minimum number of stages in an open steam distillation column with a saturated liquid feed with solute mole fraction of 0.5. The top product composition is 0.95, and % recovery and relatively volatility as given in the figure.

Clearly the results presented above are not all those obtained. The model has also been solved for open steam distillation columns where the feed is a saturated vapor. In this case the model for the system is different for the case above, and hence the solutions are also very different, although can be achieved in the same manner as above. Graphs of these solutions (in a similar format as Fig 5.1 – 5.3) are available from the author if required.

The equations for different feeds containing both liquid and vapor have not been solved yet, although the method will be analogous to the above. (The fraction of the feed in the vapor phase is required to be known in order to solve the 2-phase feed problem). While subcooled liquid or superheated vapor feeds could also be used in industrial columns, the problem becomes more complex because of the need to perform the energy balance at the feed, and thus subcooling or superheating in terms of the enthalpy relative the saturated state must also be known (and is not given a-priori in the relative volatility value). This is beyond the scope of the present study and has not been attempted.

Chapter VII
Summary

There are two studies within the present study, a study of a model of the solution mediated transformation of polymorphs, which will be used to further understand how different crystalline polymorphs convert from less stable polymorphs to more stable polymorphs, and a model of an open steam distillation column that can be used to find the reflux ratio at which a minimum of stages will be required. Both problems are very significant in the chemical industry, and also in the pharmaceutical industry for the polymorph problem.

The mathematical study of the polymorph transformation was very successful, leading to a good model of the phase transition, with all parameters but one coming from experimental measurements of the underlying mechanisms. Only the dissolution rate constant of the metastable polymorph needed to be fitted. We have fully investigated why this parameter causes difficulties, and have made conclusions about this in a full study. The work was published in Journal of Crystal Growth and also presented as a Plenary Presentation in the Asian Crystallization Technology Society symposium in 2012.

In the second problem, it was possible to model the system to find a general model between the number of stages and the reflux ratio, with the other significant variables in the systems (the feed state and composition, the top product composition, the percent recovery of the solute,…) as parameters in the model. It was also possible to find an analytical solution for the derivative of this model with respect to the reflux ratio. Setting this derivative to zero and solving for the reflux ratio gives the reflux ratio that will result in a minimum number of stages in the system. Unfortunately the analytical equation is many pages long in Maple code, and Maple (and Reduce) is unable to find a general solution for where this equation is equal to zero. However, if values are given for the parameters needed in the design of the column a numerical solution can be found for any set of conditions, and thus the minimum number of stages can be found. Some of these solutions are plotted here, and other can be requested from the author. The minimum number of stages possible for a separation is an important consideration in the design of distillation columns, as it sets a limit for possible designs, and suggests a likely number of stages to be used in a real column.

References

1. G. U. Kulkarni, P. Kumaradhas, C. N. R. Rao, Charge density study of the polymorphs of p-nitrophenol, Chem. Mater. 10 (1998) 3498-3505.
2. S. M. Reed, T. J. R. Weakley, J. E. Hutchison, Polymorphism in a conformationally flexible substituted anthraquinone; a crystallographic, thermodynamic, and molecular modeling study, Cryst. Eng. 3 (2000) 85-99.
3. H. M. Hulbert, S. L. Katz, Some problems in particle technology. A statistical mechanical formulation, Chem. Eng. Sci., 19 (1964) 555-574.
4. A. D. Randolph and M. A. Larson, Transient and steady state size distributions in continuous mixed suspension crystallizers, AIChE J., 8 (1962) 639-645.
5. A. D. Randolph, A population balance for countable entities, Can. J . Chem. Eng., 42 (1964) 280-281.
6. A. D. Randolph and M. A. Larson, Theory of particulate processes: Analysis and techniques of continuous crystallization, second ed., Academic Press, San Diego, USA.
7. J. Garside, A. Mersmann, J. Nyvlt (ed.), Measurement of Crystal Growth and Nucleation Rates, second ed., IChemE, Rugby, UK, 2002.
8. J. Schöll, D. Bonalumi, L. Vicum, M. Mazzotti, In situ monitoring and modeling of the solvent-mediated polymorphic transformation of L-glutamic acid, Cryst. Growth Des., 6 (2006) 881-891.
9. M. Trifkovic, S. Rohani, M. Sheikhzadeh, Kinetics estimation and polymorphic transformation modeling of buspirone hydrochloride, J. Cryst. Proc. Tech., 2 (2012) 31-43.
10. L. Wantha, A. E. Flood, Nucleation Kinetics of the γ-Polymorph of DL-Methionine, Chem. Eng. Technol., 35 (2012) 1024-1030.
11. L. Wantha, A. E. Flood, Crystal growth rates and secondary nucleation threshold for γ-DL-methionine in aqueous solution, J. Cryst. Growth, 318 (2011) 117-121.
12 L. Wantha, A. E. Flood, Growth and dissolution kinetics of α and γ polymorphs of DL-methionine, J. Cryst. Growth, doi:10.1016/j.jcrysgro.2011.10.064 (2012).
13. J. Cornel, C. Lindenberg, M. Mazzotti, Experimental characterization and population balance modeling of the polymorph transformation of L-glutamic acid, Cryst. Growth Des., 9 (2009) 243-252.

14. A. J. Derksen, W. J. P. van Enckevort, M. S. Couto, Behaviour of steps on the (001) face of $K_2Cr_2O_7$ crystals, J. Phys. D Appl. Phys. 27 (1994) 2580-2591.
15. P. Pantaraks, A. E. Flood, Correlation between single crystal growth rates and dissolution rates of sucrose, Chem. Eng. Trans., 1 (2002) 347-352.
16. I. A. Khaddour, L. S. M. Bento, A. M. A. Ferreira, F. A. N. Rocha, Kinetics and thermodynamics of sucrose crystallization from pure solution at different initial supersaturations, Surf. Sci., 604 (2010) 1208-1214.
17. A. VanHook, Crystallization: Theory and Practice, Reinhold, New York, USA, 1961.
18. A. A. Chernov, L.N. Rashkovich, Spiral crystal growth with nonlinear dependence of step growth rate on supersaturation; the {110} faces of KH_2PO_4 crystals in aqueous solution, J. Cryst. Growth, 84 (1987) 389-393.
19. L. Rong, T. Yamane, N. Niimura, Measurement and control of the crystal growth rate of tetragonal hen egg-white lysozyme imaged with an atomic force microscope, J. Cryst. Growth, 217 (2000) 161-169.
20. N. Kubota, M. Yokota, J. W. Mullin, Supersaturation dependence of crystal growth in solutions in the presence of impurity, J. Cryst. Growth, 182 (1997) 86-94.
21. S.-B. Zhang, M. Stepanski, J.-J. Yuan, J. Ulrich, in: A. Mersmann (ed.), Proceedings 11th Symposium on Industrial Crystallization, Garmisch-Partenkirchen, 1990, pp. 695-700.
22. S. Srisa-nga, A. E. Flood, E. T. White, The secondary nucleation threshold and crystal growth of α-glucose monohydrate in aqueous solution, Cryst. Growth Des., 6 (2006) 795-801.
23. P. Elankoven, K. A. Berglund, Contact nucleation from aqueous dextrose solutions, AIChE J., 33 (1987) 1844-1849.
24. J. Schöll, L. Vicum, M. Müller, M. Mazzotti, Precipitation of L-glutamic acid: Determination of nucleation kinetics, Chem. Eng. Technol., 29 (2006) 257-264.
25. S. Teychené and B. Biscans, Nucleation kinetics of polymorphs: Induction period and interfacial energy measurements, Cryst. Growth Des., 8 (2008) 1133-1139.
26. Threlfall and R.W. De'Ath, Metastable Zone Widths and Conformational Multiplicity, 10th International Workshop, Crystal Growth of Organic Materials, 11-14 June 2012, Limerick, Ireland (2012).